Construction and Building Materials 125 (2016) 326–336

Contents lists available at ScienceDirect

Construction and Building Materials

journal homepage: www.elsevier.com/locate/conbuildmat

Experimental and numerical study on choosing proper pulse shapers for testing concrete specimens by split Hopkinson pressure bar apparatus

Alireza Bagher Shemirani [a], R. Naghdabadi [b,c,*], M.J. Ashrafi [b]

[a] Department of Civil Engineering, Sharif University of Technology, Tehran, Iran
[b] Department of Mechanical Engineering, Sharif University of Technology, Tehran, Iran
[c] Institute for Nano-Science and Technology, Sharif University of Technology, Tehran, Iran

HIGHLIGHTS

- Using a proper pulse shaper is prerequisite for valid SHPB tests of concrete specimens.
- Numerical results validated by SHPB tests are used to provide guidelines to choose pulse shapers.
- Cross sectional area and thickness of pulse shaper is proportional to the striker bar velocity.
- Relatively small diameter and thick pulse shaper is recommended as proper one for concrete specimens.

ARTICLE INFO

Article history:
Received 16 May 2016
Received in revised form 10 August 2016
Accepted 11 August 2016

Keywords:
Split Hopkinson pressure bar
Concrete
Pulse shaper
Wave propagation
Strain rate

ABSTRACT

Dynamic behavior of concrete specimens is investigated experimentally and numerically by split Hopkinson pressure bar (SHPB) tests. In order to accurately determine dynamic properties of brittle materials such as concrete, specimens should be subjected to particular pulse loading that can be generated by using pulse shapers. Choosing proper pulse shaper dimensions helps to obtain dynamic stress equilibrium, achieve constant strain rate and minimize pulse oscillation in the concrete specimens. To this end, SHPB tests are performed for concrete specimens and effective parameters on shaping pulses such as striker bar velocity, diameter and thickness of the pulse shaper are studied experimentally and numerically. In this regard, dynamic compressive strength, modulus of elasticity, toughness and damage behavior of the concrete specimens are calculated incorrectly if improper pulse shaper is used. Numerical results validated by the experimental data are used to provide general guidelines to properly choose dimensions of the pulse shapers for the concrete specimens in the SHPB test. Results show that use of a relatively small diameter and thick pulse shaper is suggested as a proper one for testing concrete specimens. Based on the findings of this research, if a proper pulse shaper is available for testing the concrete specimen in a specified strain rate, for other strain rates the cross sectional area as well as thickness of the pulse shaper should be changed proportional to the striker bar velocity that is related to the strain rate in the specimen.

1. Introduction

Split Hopkinson pressure bar (SHPB) or Kolsky apparatus is an important experimental device for characterizing dynamic behavior of materials at high strain rates [1]. However, experimental research works [2,3] have shown that dynamic stress equilibrium and constant strain rate condition during SHPB tests are prerequisites for valid results.

In conventional SHPB test, the incident pulse has a rectangular shape with high frequency oscillations [4,5]. The high-frequency oscillations cause severe fluctuations in the dynamic stress-strain (σ-ε) curve [6,7]. In brittle specimens such as concrete, duration of effective deformation is very short under impact loading, so it is a major problem for maintaining constant strain rate and dynamic stress equilibrium. Also, the sharp rising edge of the incident pulse in the conventional SHPB test initiates undesired damage in the concrete specimens. Thus, the rising time and stress intensity of the incident pulse could be adjusted to maintain constant strain rate and dynamic stress equilibrium in a SHPB test [8]. Concrete has usually failure strain less than 1% when the

* Corresponding author at: Department of Mechanical Engineering, Sharif University of Technology, Tehran, Iran.
E-mail address: naghdabd@sharif.edu (R. Naghdabadi).

http://dx.doi.org/10.1016/j.conbuildmat.2016.08.045
0950-0618/

loading is applied too fast like in SHPB test. It is hard to obtain dynamic stress equilibrium in the concrete specimen because the specimen may fail immediately in a non-uniform manner (i.e. the front of the specimen may be shattered while the back remains intact). In order to accurately determine dynamic behavior of materials by SHPB test, several pulse shaping techniques have been utilized. Using a soft disc known as pulse shaper between the striker and incident bars is a common pulse shaping technique in SHPB apparatus. The striker bar impacts on the pulse shaper before the incident bar. It generates a non-dispersive ramp pulse that controls the shape of the loading pulse in the incident bar [9–11]. Pulse shaper absorbs high-frequency oscillations of the incident pulse and changes the rectangular-shaped incident pulse to a trapezoidal or half sinusoidal shape with a longer rise time. Slowly rising incident pulse is a preferred loading pulse to minimize effects of dispersion and inertia, which facilitates dynamic stress equilibrium in the specimen [12–14]. Other pulse shaping methods have been investigated in previous studies. Christensen et al. [15] have used conical striker bars at impact end instead of the striker to achieve ramp pulse for rock specimens. Li et al. [16,17] used a tapered or truncated cone shape striker bar on both ends to generate a half sinusoidal incident pulse shape for testing rock specimens. Ellwood et al. [18], Parry et al. [19] and Forrestal et al. [20] introduced modified SHPB apparatus which used dummy specimen and preloading bar between the striker and input bars. In order to calculate the impact properties of aramid fiber reinforced polymer confined concrete, Yang et al. [21] used H62 brass pulse shaper with thickness of 1 mm to reshape the waveform of the incident pulse. They suggested that for valid SHPB tests, pulse shapers should be used to improve the stress equilibrium in the tests. Deng et al. [22] applied a copper disk with diameter of 12 mm and thickness of 1 mm as the pulse shaper to prolong the rise time of the incident stress pulse for studying compressive behavior of cellular concretes subjected to high strain rate loadings. Performing SHPB tests, Naghdabadi et al. [23] recommended proper pulse shapers for work hardening materials such as C10200 copper and GGG60 cast iron. They suggested that thickness and cross sectional area of the pulse shaper should be changed proportional to the striker bar velocity. It has been shown that a broad range of incident pulses can be obtained by changing dimensions of pulse shaper and striking velocity. The proper material for pulse shaping depends on the mechanical characteristics of the specimen as well as velocity of the striker bar. Considering the literature on SHPB test of cement based materials such as concrete, the pulse shaper may be made of copper [3,11,22,24,25], rubber [25], stainless steel [11] and brass [21,26–29].

In previous studies [21,22,24,25], dimensions of pulse shaper for testing different concrete specimens have been determined via try and error by experimental trials solely. There is no established procedure for pulse shaper design used in testing concrete specimens. Also, in different strain rates or striker bar velocities, an identical dimension of the pulse shaper has usually been used for concrete specimens in the SHPB test. To obtain experimental results for different dimensions of pulse shaper, large number of SHPB tests should be performed. However, high costs of experiment, limitations of the measurement methods and parameter variation make it difficult to propose a procedure to choose proper pulse shapers for concrete specimen in the SHPB tests.

In this paper, employing a copper pulse shaper, effective pulse shaping parameters i.e., pulse shaper diameter (d_p) and thickness (t_p) are investigated through using the SHPB experiments and simulations by finite element software LS-DYNA. Also, dynamic behavior of concrete specimens is determined at different strain rates with and without pulse shaper. Guidelines to choose proper dimensions of pulse shaper for the concrete specimens are explained. In addition, effects of pulse shaper parameters on dynamic stress equilibrium, constant strain rate condition and pulse oscillation elimination are studied. Relations between the striker bar velocity and pulse shaper dimension are obtained. Finally, effects of different striker bar lengths on incident pulse are studied. To this end, the paper is organized as follows; in Section 2, we briefly review pulse shaped SHPB apparatus; concrete specimens preparation, also static and dynamic tests of the concrete specimens. In Section 3, simulations of SHPB test are explained. In Section 4, experimental and numerical methodologies for choosing proper pulse shapers to test concrete specimens are discussed. Finally in Section 5 conclusions are drawn.

2. Experimental details

2.1. Pulse shaped SHPB apparatus

To determine the dynamic compressive strength of concrete, a SHPB test is required. SHPB test apparatus consists of a gas gun as launching system, a striker bar, an incident bar, a transmission bar and a data acquisition system (Fig. 1) [23].

The gas gun is used to launch the striker bar impacting on the incident bar. Generating a half sinusoidal shaped pulse; the concrete specimen is sandwiched between the incident and transmission bars. According to wave impedance mismatch between the specimen and bars, part of the compression wave is reflected back in the incident bar while the rest transmits in the transmission bar. Identical strain gauges are attached on the mid-point of the incident and transmission bars to measure incident (ε_I), reflected (ε_R) and transmitted (ε_T) strain pulses (Fig. 2) [12,23]. Using one-dimensional (1-D) wave theory, strain rate ($\dot{\varepsilon}_s$), strain (ε_s) and stress (σ_s) in the specimen can be calculated [30]:

$$\sigma_s(t) = \frac{A_b E_b}{A_s}\varepsilon_T(t) \tag{1}$$

$$\dot{\varepsilon}_s(t) = \frac{C_b}{h_s}\{\varepsilon_I(t) - \varepsilon_R(t) - \varepsilon_T(t)\} \tag{2}$$

$$\varepsilon_s(t) = \frac{-2C_b}{h_s}\int_0^t \varepsilon_R(t)dt \tag{3}$$

where t and A_b are time and cross sectional area of the incident and transmission bars A_s and h_s are considered as cross sectional area and thickness of the specimen. Moreover, E_b and C_b denote Young modulus and wave velocity in the pressure bars, respectively. Table 1 shows specifications of the SHPB apparatus utilized for testing concrete specimens in the present work. The incident, transmission and striker bars have the same diameter of 63 mm and lengths of 2.5, 1.5 and 0.3 m, respectively.

Brittle specimens should be subjected to particular stress pulse loadings such that deform uniformly under a dynamic stress equilibrium state at a constant strain rate. In most cases, a trapezoidal incident pulse does not facilitate achievement of these experimental conditions. Therefore, in order to produce a ramp incident pulse, a pulse shaping technique should be used in SHPB [31]. For concrete specimens, pulse shaping improves the incident pulse profile. The pulse shaper is attached with grease between the striker and incident bars as shown in Fig. 3.

A half sinusoidal incident pulse is suitable for testing brittle materials with linear stress-strain behavior [18]. In this study, a C10200 copper disc with diameter of 12 or 24 mm and thickness of 1 or 2 mm is used to reshape the incident pulse. Chemical composition in weight percentage and quasi-static mechanical properties of the C10200 copper are summarized in Table 2.

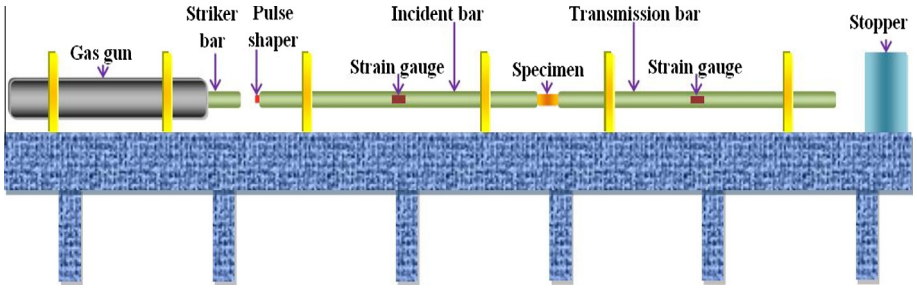

Fig. 1. Schematic of the pulse shaped SHPB test apparatus [23].

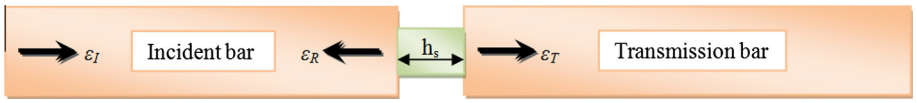

Fig. 2. Schematic of the strain pulses propagation in the SHPB test.

Table 1
Specifications of SHPB apparatus for testing concrete specimens.

Bar	Length (mm)	Diameter (mm)	Material	Mass density ρ (kg/m^3)	Young modulus E_b (GPa)	Poisson ratio υ	Wave velocity C_b (m/s)
Striker bar	300	63	Aluminum 7075	2810	71.7	0.33	5050
Incident bar	2500	63	Aluminum 7075	2810	71.7	0.33	5050
Transmission bar	1500	63	Aluminum 7075	2810	71.7	0.33	5050

Fig. 3. Copper pulse shaper located between the striker and incident bars.

2.2. Preparation of concrete specimens

Concrete mixtures consist of normal Portland cement (ASTM type A), crushed coarse aggregates with a maximum size of 10 mm and natural sand. Both coarse and fine aggregates grading satisfy requirements of ASTM C33/C33M-16 [32]. Specific gravity of aggregates is 2.8 and 2.5 for coarse aggregates and sand, respectively. A polycarboxylate super plasticizer (water-reducing) with a specific gravity of 1.1 is used in the admixture. The plasticizer classified as ASTM C494 type A, increases workability, improves cohesiveness and reduces segregation [33]. Proportions of the concrete mixture are reported in Table 3.

According to the maximum aggregate size and diameter of SHPB bars, the concrete specimen diameter is chosen to be 62 mm. Moreover, to minimize inertia effects, aspect ratio length/-diameter of the specimen is 1.5 [34]. All specimens are cured at 20 ± 5 °C and 100% relative humidity for more than 28 days.

2.3. Concrete specimen static test

With a servo-hydraulic material test system (MTS), the compressive strength test is carried out based on ASTM C39 at 28 days after the date of mixing. Strain rate of about $5 * 10^{-5}$ (s^{-1}) is considered to satisfy the requirement of ASTM C39/C39M-16 [35]. According to ASTM C469, the elastic modulus is determined at a point corresponding to 50% of ultimate loading [36]. Quasi-static compressive strength ($f'_c = 48.51$ MPa) and shear modulus ($G = 8.19$ GPa) are obtained from the static compressive test and maximum tensile strength is calculated with ACI 318-14 [37] relation ($T = 0.56 f'^{0.5}_c$).

2.4. Concrete specimen dynamic test

To study the effects of pulse shaper dimensions on the incident pulse shape, we perform several SHPB tests on the concrete specimens by employing different pulse shaper thicknesses and

Table 2
Chemical composition and mechanical properties of the C10200 copper.

Chemical composition (Weight %)	Cu	Al	Ni	Fe	S	Pb	Zn	Mg	Si
	~99.98	0.0078	0.0033	0.0018	0.0014	0.0014	0.0009	0.00011	<0.0004
Mechanical properties	Mass density 8960 kg/m^3		Young modulus 129 GPa		Poisson ratio 0.3		Yield stress 225 MPa		Failure strain 16%

Table 3
Mix proportion and workability of the concrete.

W/C	Cement (kg/m^3)	Water (kg/m^3)	Coarse aggregates (kg/m^3)	Sand (kg/m^3)	Super Plasticizer (kg/m^3)	Slump (mm)	Mass density ρ (kg/m^3)
0.35	470	170	1100	600	5.5	50	2193

diameters as well as tests without pulse shapers. In the SHPB test, the striker bar velocity (V_s) and its length (L_s) are 19 m/s and 300 mm, respectively. To minimize the end friction confinement during SHPB test, the concrete specimens are attached to the incident and transmission bars with a very thin layer of grease. We perform experiments without pulse shaper and with other pulse shaper dimensions such as $t_p = 1$, $d_p = 12$ mm, $t_p = 1$, $d_p = 24$ mm and $t_p = 2$, $d_p = 12$ mm to show the effects of the pulse shaper dimensions on the dynamic behavior of the concrete specimens. To ensure that the SHPB test results are valid, for each case, three tests are done. The results of these experiments will be shown and discussed in Sections 3 and 4.

There are different methods to define the representative strain rate in the SHPB test such as averaging strain rate that is defined as the total strain divided by the total loading period [38], and average value of the strain rate histories over the time duration when the stress level exceeds 80% of the peak stress [39]. These averaging methods can't represent the actual strain rate because of brittle failure occurrence in the concrete specimens [25]. In another method the representative strain rate in a SHPB test is the strain rate at the failure point of the concrete specimens [25]; that has been used in the current study. It is noted that averaging strain rate is needless when proper pulse shaper is used. Achievement of constant strain rate condition during SHPB tests by using a proper pulse shaper leads to the same representative strain rate in these different methods.

3. Simulation of SHPB test

Using experimental data, SHPB test simulations are validated for different pulse shapers. SHPB test are simulated to choose the proper pulse shaper and predict pulse shaper effects for the concrete specimen. In this simulation, the pulse shaper, concrete specimen, striker, incident and transmission bars are considered in the modeling. For simulations, finite element software LS-DYNA with an axisymmetric model is used (Fig. 4).

In this study, the finite element model contains 21,600 four-node quadrilateral elements where sizes of elements are smaller than 2.5 mm * 2.5 mm. The model mesh size is fine enough to guarantee the mesh independence and numerical convergence of the solution.

A surface to surface contact is defined between interfaces of different parts in the model. For the initial condition, the impact velocity of the striker bar is considered. Material model for different parts are defined as follow:

- Elastic (MAT_001) for the incident and transmission bars
- Plastic-kinematic (MAT_003) for the pulse shaper
- Johnson-Holmquist-Concrete (JHC) (MAT_111) for the concrete specimen

Table 4
The material parameters for the pulse shaper (plastic-kinematic).

Mass density ρ. (kg/m^3)	Young modulus E (GPa)	Poisson ratio υ	Yield stress σ_y (MPa)	Hardening parameter β	Tangent modulus E_{tan} (MPa)
8960	129	0.3	225	1	656

The plastic-kinematic model is an appropriate model for isotropic and kinematic hardening plasticity with the option of including strain rate effects. The material parameter specifications of the plastic-kinematic model (Table 4) are measured by test on the copper pulse shaper [23]. For simulation of the concrete specimens subjected to high strain rates and high pressures, JHC model is selected [40]. In this model, equivalent strength is expressed as a function of pressure, strain rate, and damage in the following form [41]:

$$\sigma^* = [A(1-D) + BP^{*n}][1 + C\ln\dot{\varepsilon}^*] \tag{4}$$

where the von Mises flow stress (σ) and pressure (P) are normalized by the quasi-static uniaxial compressive strength (f_c') such that $\sigma^* = \sigma/f_c'$ and $P^* = P/f_c'$. Also, term $\dot{\varepsilon}^* = \dot{\varepsilon}/\dot{\varepsilon}_0$ is the dimensionless equivalent strain rate. A, B, C and n are material constants. The damage (D) is accumulated as a function of the plastic volumetric strain ($\Delta\mu_p$) and equivalent plastic strain ($\Delta\varepsilon_p$) expressed as:

$$D = \sum \frac{\Delta\varepsilon_p + \Delta\mu_p}{D_1(P^* + T^*)^{D_2}} \tag{5}$$

where $T^* = T/f_c'$ is the normalized maximum tensile hydrostatic pressure (T), D_1 and D_2 are material constants. The pressure (P) for fully dense material is a function of the modified volumetric strain ($\overline{\mu}$) expressed in the form:

$$P = K_1\overline{\mu} + K_2\overline{\mu}^2 + K_3\overline{\mu}^3 \tag{6}$$

where K_1, K_2 and K_3 are material constants. Based on locking volumetric strain (μ_{Lock}), the modified volumetric strain ($\overline{\mu}$) is defined as:

$$\overline{\mu} = \frac{\mu - \mu_{Lock}}{1 + \mu_{Lock}} \tag{7}$$

Equation of state (EOS) is used to mathematically describe the behavior of the material for all possible states of stress. For concrete, EOS includes elastic, crushable transition and locked regions [40,41]. To accurately determine parameters of EOS for concrete, specific experimental tests such as quasi-static uniaxial tension (splitting cylinder), uniaxial compression and tri-axial stress and flyer plate impact tests are required. Because of limitations on performing these tests, in this work the EOS parameters (Table 5) are obtained according to relations suggested by Tai et al. [42]. The concrete specifications such as mass density, shear modulus,

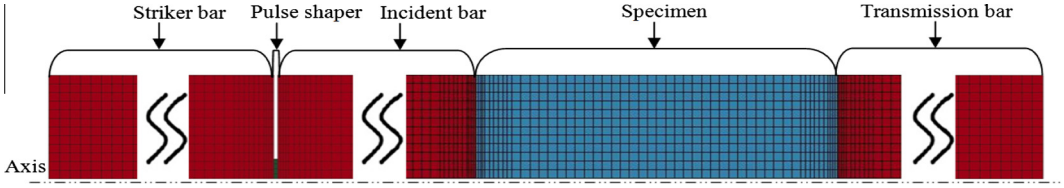

Fig. 4. Model of SHPB test in LS-DYNA.

Table 5
Equation of state constants for the concrete specimens [42].

Crushing volumetric strain μ_{crush}	Locking pressure P_{Lock} (GPa)	Locking volumetric strain μ_{Lock}	Pressure constants		
			K_1	K_2	K_3
0.00058	1.05	0.1	17.4	38.8	29.8

Table 6
The concrete specifications.

Mass density ρ (kg/m^3)	Shear modulus G (GPa)	Quasi-static compressive strength f'_c (MPa)	Maximum tensile hydrostatic pressure T (MPa)	Crushing pressure P_c (MPa)
2193	8.18	48.51	3.9	16.2

Table 7
Material parameters for the concrete (JHC).

Material coefficients				Damage constants		Amount of plastic strain before fracture
A	B	C	n	D_1	D_2	ε_{fmin}
0.55	1.64	0.01	0.69	0.1	1	0.01

quasi-static compressive strength and maximum tensile hydrostatic pressure (Table 6) are obtained from static tests (Section 2.3). Other concrete parameters of JHC model (Table 7) are obtained from SHPB test (Section 2.4) with pulse shaper $t_p = 2$ and $d_p = 12$ mm for $V_s = 19$ m/s.

In Fig. 5 validation of the simulation results with the experiment data for different tests are shown. Fig. 6 shows experiment data of the concrete stress-strain curve for different tests that compared with the simulation results. It is observed that the simulation results are in good agreement with the experiment data.

4. Results and discussion

In this section, the experimental data and simulation results are used to determine dimensions of the proper pulse shaper. Also, effects of the pulse shaper parameters on dynamic stress equilibrium, strain rate condition and minimum dispersion effects are investigated. Fig. 7A, shows incident, reflected and transmitted strains for the concrete specimens without pulse shaper. Fig. 7B–D show strains using pulse shapers with $t_p = 1$, $d_p = 12$ mm, $t_p = 1$, $d_p = 24$ mm and $t_p = 2$, $d_p = 12$ mm, respectively.

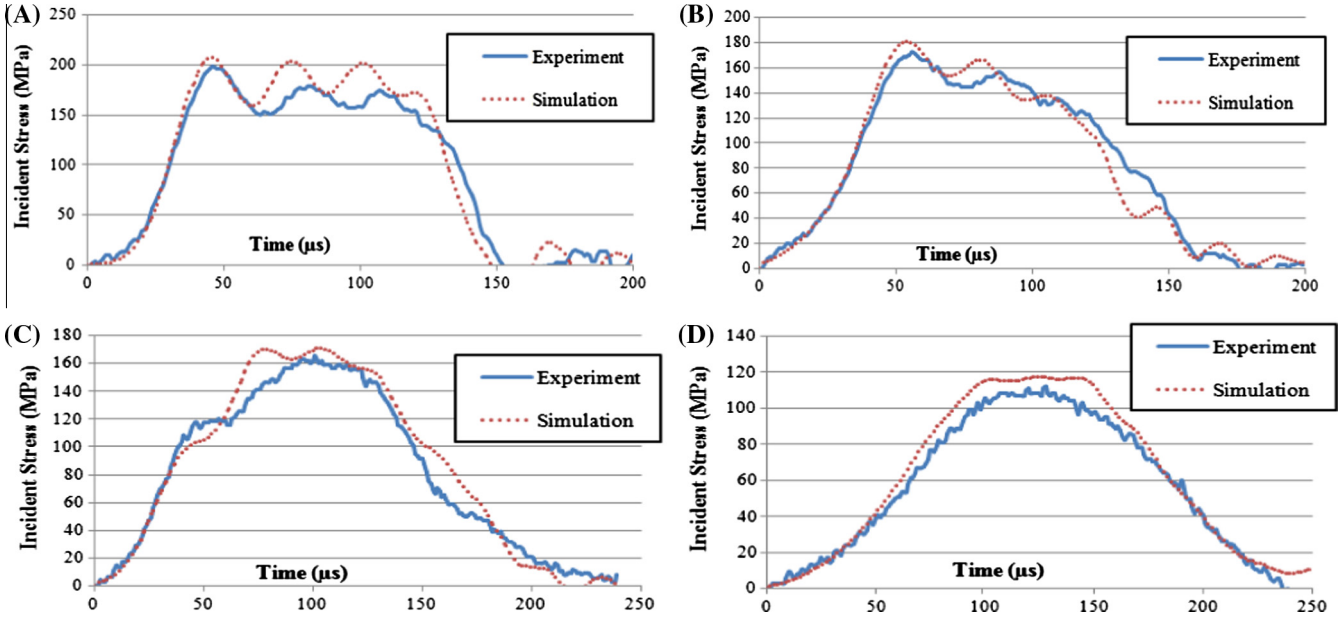

Fig. 5. Incident stress for $V_s = 19$ m/s: (A) without pulse shaper, using pulse shapers with (B) $t_p = 1$, $d_p = 12$ mm, (C) $t_p = 1$, $d_p = 24$ mm and (D) $t_p = 2$, $d_p = 12$ mm.

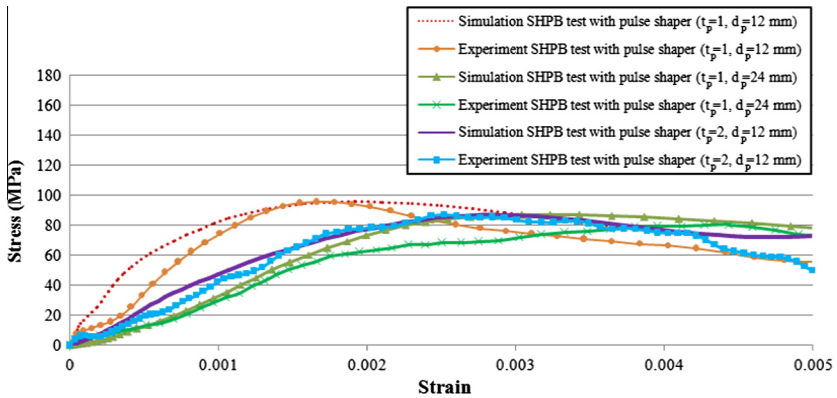

Fig. 6. Stress-strain curve for the concrete specimens with $V_s = 19$ m/s and different pulse shaper dimensions.

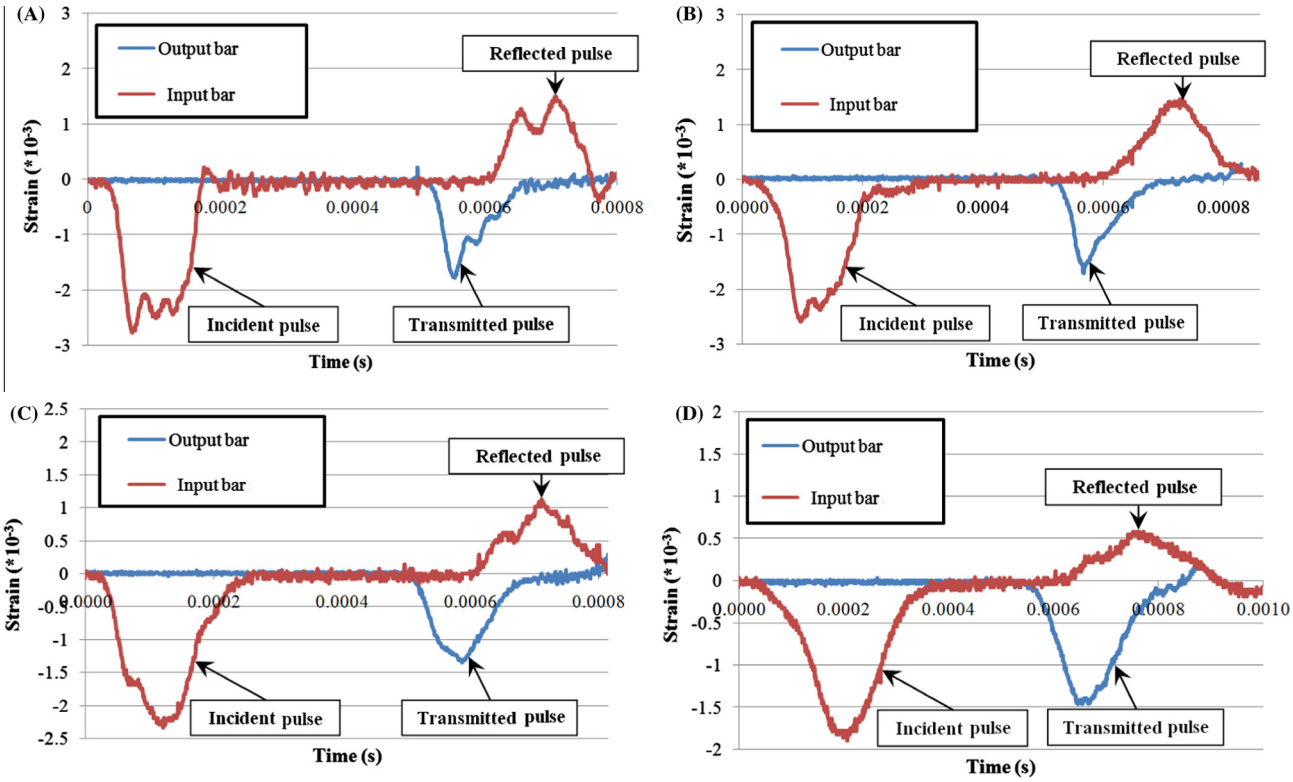

Fig. 7. Incident, reflected, and transmitted strains in SHPB tests: (A) without pulse shaper, using pulse shapers with (B) t_p = 1, d_p = 12 mm, (C) t_p = 1, d_p = 24 mm and (D) t_p = 2, d_p = 12 mm.

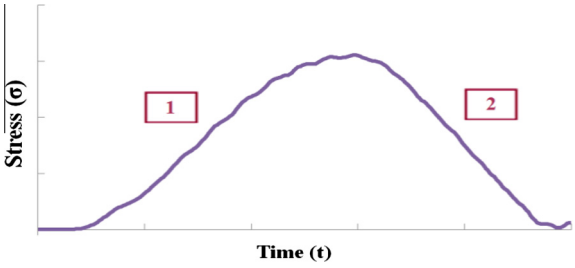

Fig. 8. Typical incident stress pulse: (1) increasing and (2) decreasing parts.

A half sinusoidal incident pulse with relatively long rise time is a desirable incident pulse shape that could follow the concrete specimen stress-strain behavior as shown in Fig. 7D. The appropriate shaped incident pulse, for the concrete specimens as depicted in Fig. 8 consists of a half sinusoidal pulse which is described as:

1. Increasing part: deformation of the pulse shaper during loading.
2. Decreasing part: unloading of the pulse shaper

The duration of each part depends on velocity of the striker bar (V_s) as well as thickness (t_p) and diameter (d_p) of the pulse shaper. The duration of each part increases when the pulse shaper thickness increases and/or pulse shaper diameter decreases as shown in Fig. 7.

4.1. Dynamic stress equilibrium

Stress uniformity along the specimen length (i.e. dynamic stress equilibrium) is a prerequisite for valid SHPB tests [43]. With identical incident and transmission bar cross sections, dynamic stress equilibrium is achieved i.e. $\varepsilon_I + \varepsilon_R = \varepsilon_T$. However, it is impossible to reach absolute dynamic stress equilibrium when impedance mismatch exists between the concrete specimen and pressure bars [44]. Since concrete failure strain is less than 1%; before achieving dynamic stress equilibrium, concrete specimen is damaged under the effect of the ascent part of the half sinusoidal incident pulse.

Fig. 9 shows dynamic equilibrium of experimental data with and without pulse shaper. As shown in the figure, sum of the incident and reflected pulses coincide approximately with the transmitted pulse when the pulse shaper is used.

In order to investigate dynamic stress equilibrium, the dynamic stress non-equilibrium factor $\delta(T_R)$ introduced by Su et al. [29] is used in the following form:

$$\delta(T_R) = \frac{\int_0^{T_R}[\varepsilon_I(t) + \varepsilon_R(t) - \varepsilon_T(t)]dt}{\int_0^{T_R}\varepsilon_T(t)dt} \quad (8)$$

For a better equilibrium, $\delta(T_R)$ should be minimized with respect to T_R, where T_R is time. T_R at which $\delta(T_R)$ = 5% is defined as the moment that specimen reaches to dynamic stress equilibrium. The rise time of the incident pulse should be prolonged enough that the concrete specimen reaches dynamic stress equilibrium before the onset of damage. For different pulse shapers, $\delta(T_R)$ curves are demonstrated in Fig. 10. As an example, for pulse shaper with 12 mm diameter and 2 mm thickness, it is seen that equilibrium state is achieved before the specimen failure; i.e. $\delta(T_R)$ = 5% is achieved at about 55 μs and the failure occurs at 120 μs. For the same pulse shaper the incident pulse duration is about 250 μs and the rise time of the shaped pulse falls at 120 μs as shown in Fig. 9D. In other words, sufficient time is provided for the specimen to achieve equilibrium state at early stage of dynamic loading during the test process.

With the other pulse shapers, $\delta(T_R)$ is larger than that of the pulse shaper with 12 mm diameter and 2 mm thickness. Therefore, using no or improper pulse shaper, the dynamic stress equilibrium

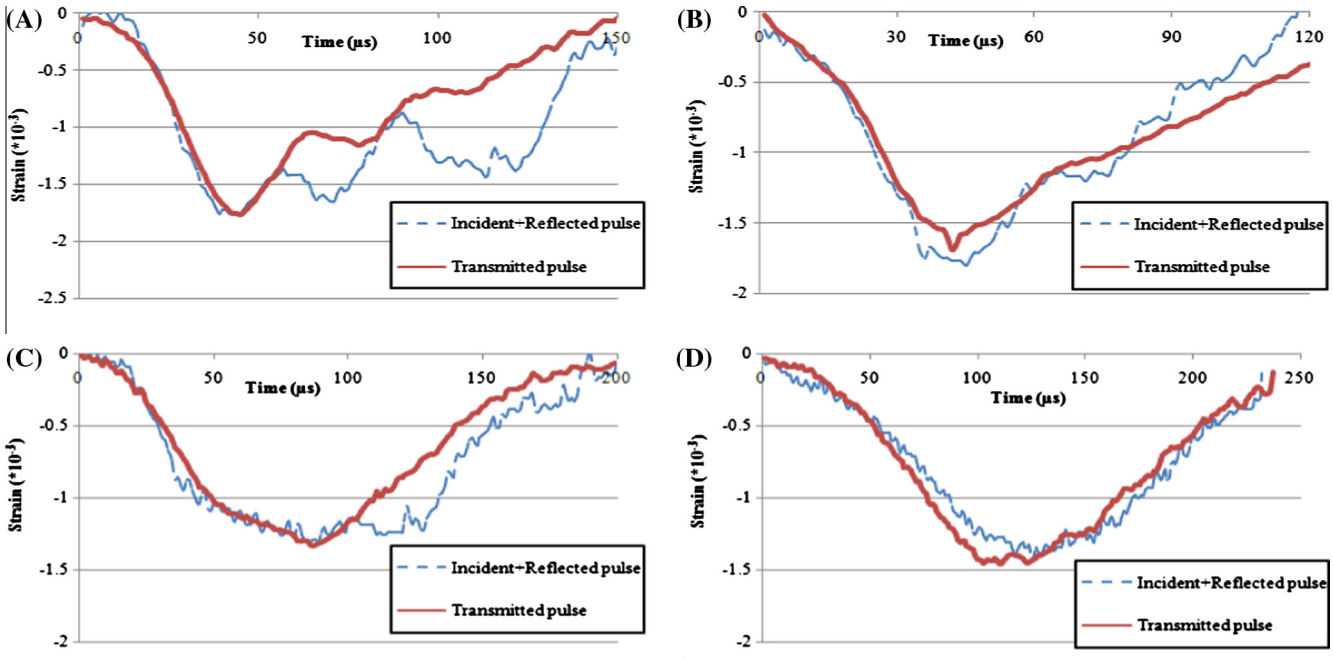

Fig. 9. Dynamic equilibrium (V_s = 19 m/s): (A) without pulse shaper, using pulse shapers with (B) t_p = 1, d_p = 12 mm, (C) t_p = 1, d_p = 24 mm and (D) t_p = 2, d_p = 12 mm.

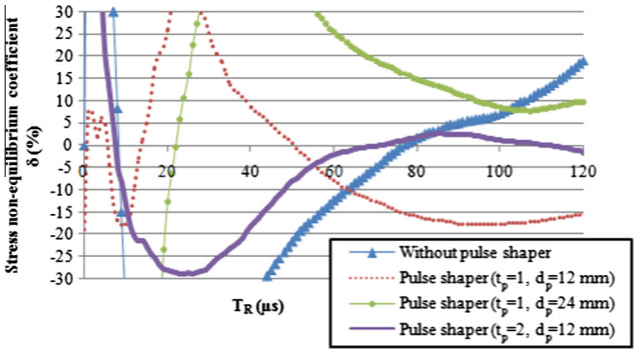

Fig. 10. Stress non-equilibrium coefficient for the specimens with different pulse shapers in SHPB tests.

is not achieved in the specimen. It is concluded that in order to achieve the dynamic stress equilibrium, a pulse shaper with relatively large thickness is needed.

4.2. Constant strain rate condition

Concrete is sensitive to strain rate [25,45]; constant strain rate condition in the specimen is required to obtain concrete dynamic behavior accurately. This condition depends on the rise time of the incident pulse. The slope rise of the incident pulse can induce premature failure of the concrete specimen. An approximately constant strain rate is achieved, when a plateau appears in the reflected pulse versus time curve. For different thickness and diameter of the pulse shaper, the reflected strains are demonstrated in Fig. 11. Such constant strain rate may be achieved through the adjustment of the striker bar velocity and dimensions of the pulse shaper. A pulse shaper with certain diameter can only offer one optimal constant strain rate for a certain striker bar velocity [46]. Assuming the dynamic stress equilibrium in the concrete specimen and substituting Eqs. (1) and (2) into (3), we obtain:

$$E_b A_b \varepsilon_I(t) - A_s \sigma_s(t) = \frac{h_s E_b A_b}{2C_b} \dot{\varepsilon}_s(t) \tag{9}$$

In order to achieve a constant strain rate in the specimen, the incident pulse should be proportional to the stress in the specimen. When the pulse shaper diameter is decreased, the reflected strain remains approximately constant. The constant strain rate condition is obtained through relatively small diameter of the pulse shaper. On the other hand, a relatively small thickness of the pulse shaper increases the strain rate in the concrete specimens. Also, a relatively large thickness pulse shaper helps to achieve the

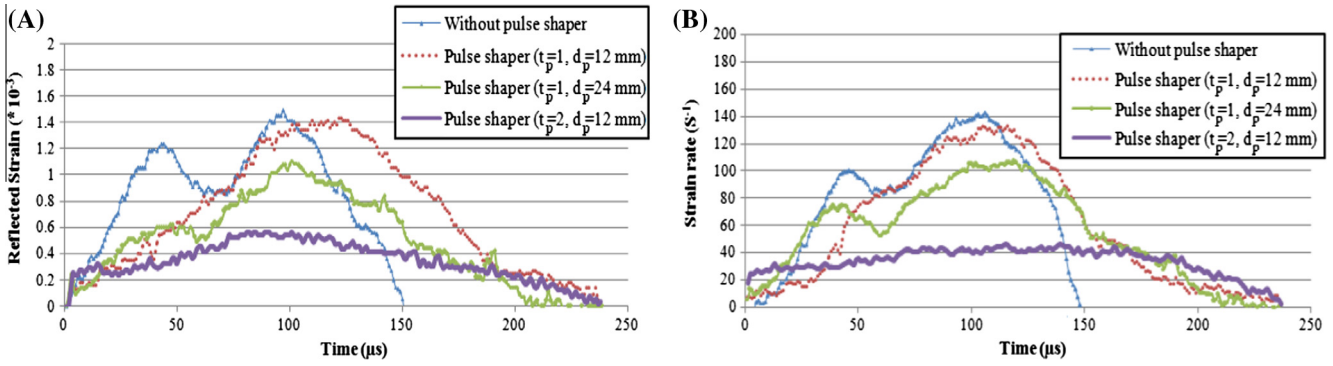

Fig. 11. (A) Reflected strain pulse, (B) strain rate curves in SHPB experiment with different pulse shapers for V_s = 19 m/s.

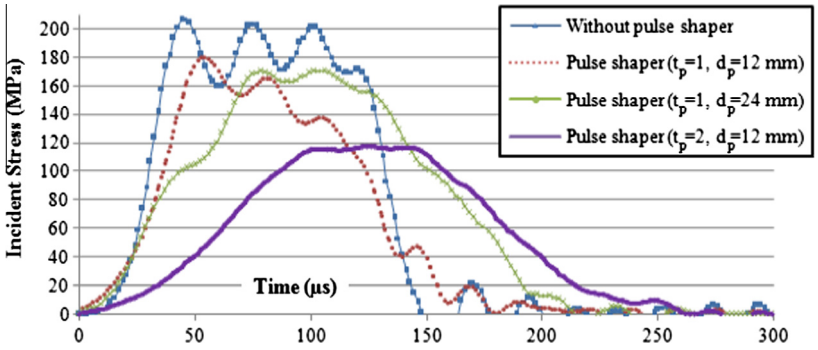

Fig. 12. Effect of thickness and diameter of different copper pulse shapers on the shape of simulated incident stress pulse for V_s = 19 m/s.

Table 8
Results for concrete specimens in static and high strain rate tests for V_s = 19 m/s.

Type of test	Pulse shaper dimension	Strain rate (S^{-1})	Compressive strength (f'_c) (MPa)	Elastic modulus (E) (GPa)	Toughness (J/cm^3)
Static	–	$5 * 10^{-5}$	48.51	26.82	0.047
SHPB test without pulse shaper	–	81.97	102.36	45.80	0.538
SHPB test with pulse shaper	t_p = 1, d_p = 24 mm	63.03	80.25	27.18	0.421
	t_p = 1, d_p = 12 mm	65.95	95.60	46.90	0.503
	t_p = 2, d_p = 12 mm	43.53	86.92	38.92	0.218

dynamic stress equilibrium. Satisfying these requirements leads to trade off between the diameter of the pulse shaper and striker bar velocity that is related to the strain rate in the specimen, which will be discussed in Section 4.5.

4.3. Minimum dispersion effects

The oscillation of the stress pulses in the concrete specimen is due to the dispersion of these pulses in the bar system. The oscillation of the incident pulse causes oscillation of the reflected and transmitted pulses, correspondingly. Hence, the test results of SHPB calculated with the incident, reflected and transmitted pulses will be deviated from true behavior [47]. Plastic deformation of the pulse shaper filters out high frequency oscillations of the incident pulse. The effect of thickness and diameter of the pulse shaper on the shape of simulated incident stress pulse is presented in Fig. 12. The simulation results show that use of a proper pulse shaper generates a half sine pulse that can effectively minimize the dispersion of the stress pulse, as shown in Fig. 12. Also, the dispersion effects of the stress pulse generated without pulse shaper is remarkable.

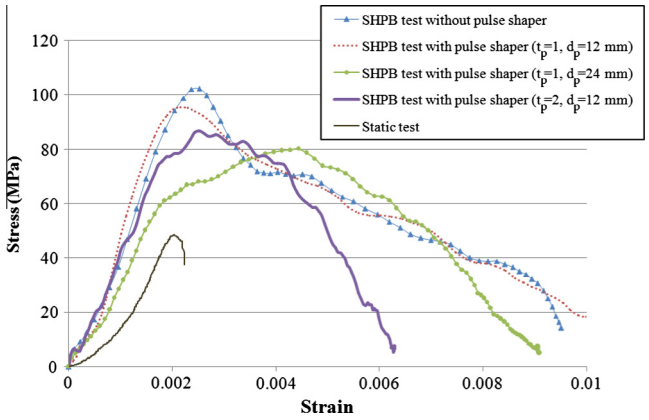

Fig. 13. Stress-strain curve for concrete specimens with different pulse shapers for V_s = 19 m/s.

4.4. Compressive strength, modulus of elasticity and toughness

Since the concrete specimens experience brittle failure, better bonding of aggregates ensures more effective stress transmission between matrices. Stress-strain curve at high strain rates is different from the static condition such that, the slope of the descending portion of the curve decreases. Fig. 13 shows the stress-strain curve of the concrete specimen under dynamic loading tests with different pulse shapers. Also, the results for these tests are presented in Table 8. As shown in Fig. 13, damage parts of the curves are sensitive to the pulse shaper dimensions. Using a relatively small diameter and thick pulse shaper, more damage is induced in the concrete specimens. It is concluded that the dynamic compressive strength of a given concrete specimen decreases by using different pulse shapers because of decreasing the strain rate. Also, diameter of the pulse shaper is more effective than its thickness on the dynamic compressive strength. Moreover, dynamic elastic modulus decreases by using pulse shapers. Area under full stress-strain curve is considered as toughness of the concrete specimens. Thus, toughness is overestimated if improper pulse shaper is used. With a relatively small diameter and thick pulse shaper (t_p = 2, d_p = 12 mm) toughness is 0.218 (J/cm^3). Increase of the diameter or decrease of the thickness of the pulse shaper results in higher values for toughness that is fairly equal to the toughness in no pulse shaper case (Table 8).

Different concrete failure patterns may occur in SHPB test such as: unbroken with micro cracks, edge crack and edge broken as well as partially broken and grinded [27]. All these dynamic failure patterns develop for different strain rates. The grinding pattern dissipates enormous amount of impact energy, so the proper pulse shaper should be used to make the grinded failure pattern as the major fracture pattern. Fig. 14 shows the failure pattern of the concrete specimen.

When concrete specimens are subjected to quasi-static loading, most of the visible cracks propagate through the mortar and interfacial transaction zone (ITZ) between the aggregates (Fig. 14B). Increasing the strain rate, more inner micro-cracks propagate in the ITZ. Due to changing the crack paths, the crack length is

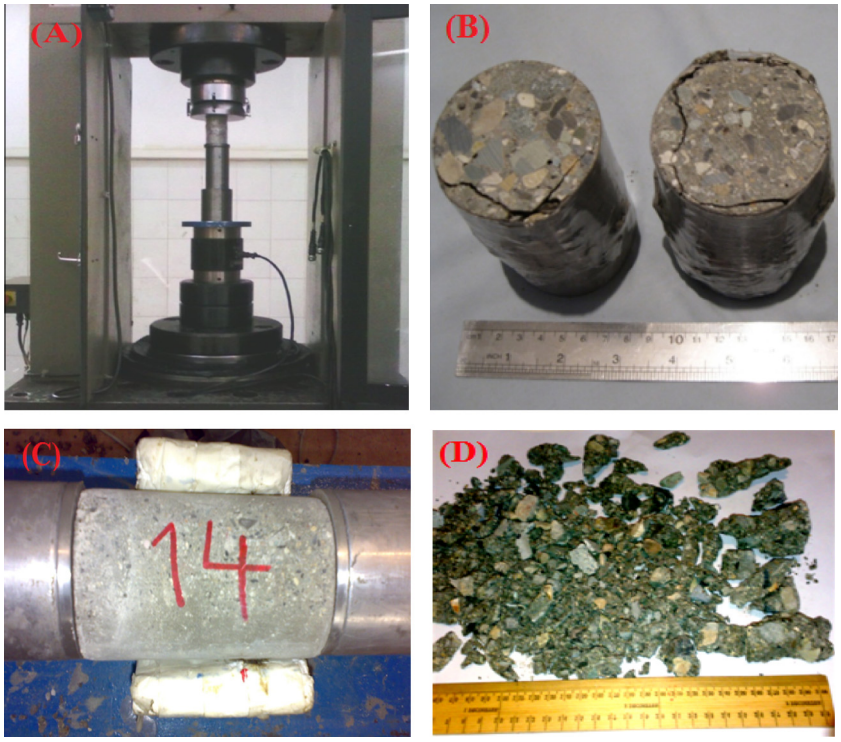

Fig. 14. (A) Typical concrete specimen before quasi-static test, (B) failure pattern after quasi-static test, (C) typical concrete specimen before SHPB test, (D) failure pattern after SHPB test.

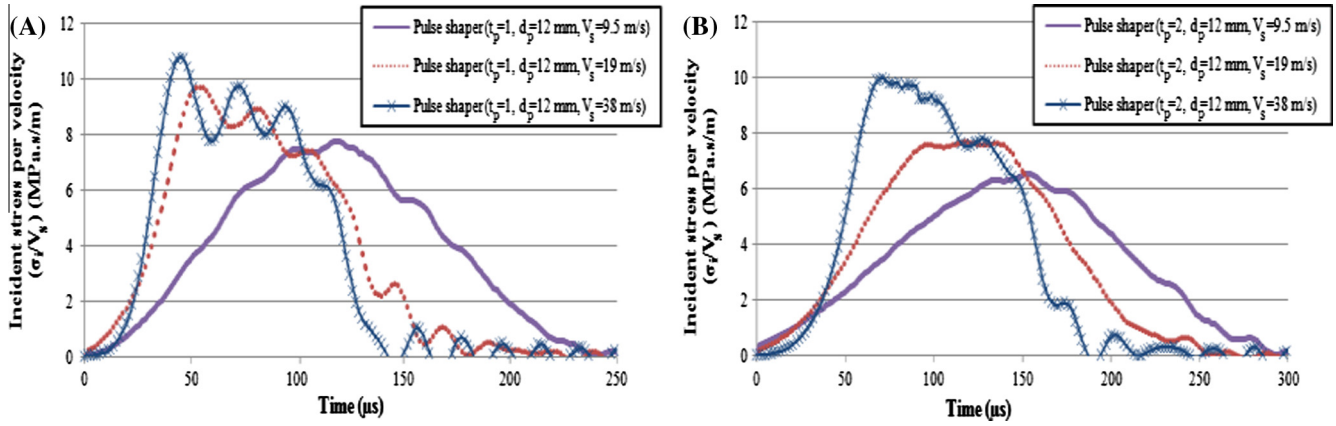

Fig. 15. Striker bar velocity effect on the normalized incident stress using pulse shapers with (A) t_p = 1, d_p = 12 mm and (B) t_p = 2, d_p = 12 mm (V_s = 9.5, 19 and 38 m/s).

shortened. Thus, more energy is consumed by generating more cracks in the mortar matrix, ITZ and aggregates that leads to fracture of the specimen into smaller fragments (Fig. 14D). In such case, complete failure of the specimen occurs with more cracks.

4.5. Striker bar velocity effect

In SHPB test the strain rate in the concrete specimen is governed by the striker bar velocity. Simulation results are used to obtain relations between the striker bar velocity and strain rate. Fig. 15 presents the normalized incident stress with respect to the striking velocity (σ_i/V_s). Based on the simulation results, the rise time of the incident stress is increased by reduction of the striker bar velocity.

Investigating different striker bar velocities with scaled pulse shaper dimensions such as diameter and thickness, we obtain approximately the same normalized incident stress curves (Fig. 16). For this purpose, thickness (t_p) and square of diameter

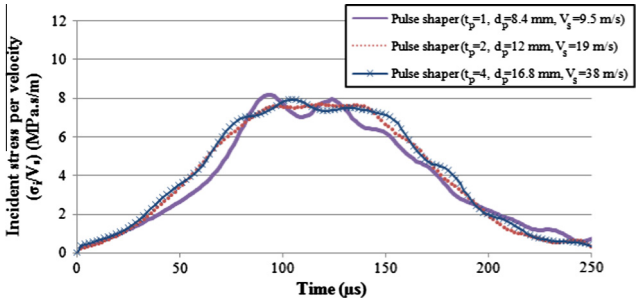

Fig. 16. Normalized incident stress for different pulse shaper dimensions per the striker bar velocities.

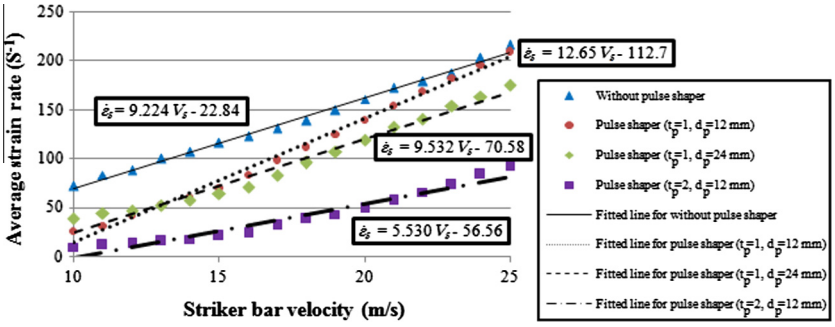

Fig. 17. Strain rate ($\dot{\varepsilon}_s$) versus the striker bar velocity.

(d_p^2) of the pulse shaper should be changed proportional to the striker bar velocity. This means that for different striker bar velocities, the ratios t_p/V_s and d_p^2/V_s should remain constant. However, the pulse shaper material should plastically deform under the striker bar velocity and diameter of the deformed pulse shaper should be smaller than the diameter of the incident bar.

Fig. 17 shows the simulation results for strain rate versus the striker bar velocity with and without pulse shaper. In this figure, various strain rates in range of 10–200 (s^{-1}) are obtained by changing the striker bar velocity between 10 and 25 (m/s). The relationship between strain rate, $\dot{\varepsilon}_s$ (s^{-1}), and the striker bar velocity, V_s (m/s), is expressed by Eq. (10). Using this equation, it is easier to select the striker bar velocity for achieving specific strain rate for different pulse shaper dimensions. As shown in Fig. 17, it is noted that strain rates more than 100 (s^{-1}) can't be achieved with pulse shaper of dimension t_p = 2, d_p = 12 mm.

$$\begin{aligned}
&\dot{\varepsilon}_s = 9.224V_s - 22.84; && \text{without pulse shaper}\\
&\dot{\varepsilon}_s = 9.532V_s - 70.58; && \text{using pulse shaper } (t_p = 1, d_p = 24 \text{ mm})\\
&\dot{\varepsilon}_s = 12.65V_s - 112.7; && \text{using pulse shaper } (t_p = 1, d_p = 12 \text{ mm})\\
&\dot{\varepsilon}_s = 5.530V_s - 56.56; && \text{using pulse shaper } (t_p = 2, d_p = 12 \text{ mm})
\end{aligned} \tag{10}$$

4.6. Striker bar length effect

Effects of different striker bar lengths are analyzed in this section. In the SHPB test for concrete specimens, the incident pulse duration is dependent on the striker bar length. Fig. 18 shows, results of incident stress shapes obtained by simulation for different striker bar lengths. In this figure, the pulse shapers thickness are 1 and 2 mm, the pulse shaper diameter is 12 mm and the striker bar velocity is chosen to be 19 m/s. It is found that the incident pulse duration extends by increasing the striker bar length. Increasing the striker bar length helps achieving uniform stress and strain in the concrete specimens before the onset of damage. As shown in Fig. 18B, increase of the pulse shaper thickness and striker bar length almost damps the high frequency oscillations of the incident pulse.

5. Conclusions

In this paper, selection of proper pulse shapers for testing concrete specimens by SHPB test is studied experimentally and numerically. Effects of the pulse shaper on the incident pulse shape, compressive strength, modulus of elasticity, toughness and damage behavior of the concrete are investigated. Considering the experimental data and simulation results, the following conclusions are made:

1. Dynamic stress equilibrium, constant strain rate condition and minimum dispersion effects in the concrete specimens during SHPB test are prerequisites for valid results, which can be provided by using a proper pulse shaper. A relatively small diameter and thick pulse shaper is recommended as a proper pulse shaper for testing the concrete specimens.
2. Using proper pulse shapers increase the rise time of the incident pulse. The rise time of the incident pulse increases by increasing the pulse shaper thickness and/or decreasing the pulse shaper diameter as well as the striker bar velocity.

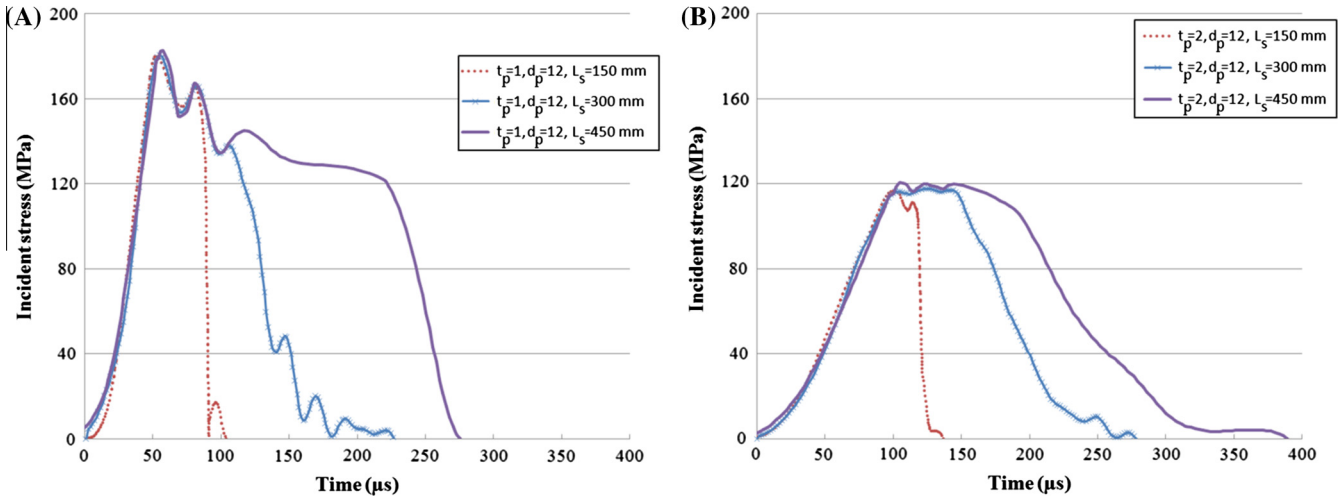

Fig. 18. Striker bar length effect on the incident stress using pulse shapers with (A) t_p = 1, d_p = 12 mm and (B) t_p = 2, d_p = 12 mm and striker bar length L_s = 150, 300 and 450 mm (V_s = 19 m/s).

3. Various incident shaped pulses are generated by changing dimensions of the pulse shaper. It is suggested that if a proper pulse shaper is available for testing concrete specimens in a specified strain rate, for other strain rates the cross sectional area as well as thickness of the pulse shaper is proportional to the striker bar velocity. Using this suggestion, we omit the try and error process for choosing dimensions of the proper pulse shaper for different strain rates in the SHPB test to obtain valid data for concrete specimens.

Acknowledgement

This research has been supported by the Impact Mechanics and Penetration Laboratory (IMPLab) of Mechanical Engineering Department, Sharif University of Technology which is gratefully acknowledged.

References

[1] C.A. Ross, P.Y. Thompson, J.W. Tedesco, Split-Hopkinson pressure-bar tests on concrete and mortar in tension and compression, ACI Mater. J. 86 (5) (1989) 475–481.
[2] C.E. Franz, P.S. Follansbee, W.J. Wright, New experimental techniques with the split Hopkinson pressure bar, in: In the 8th International Conference on High Energy Rate Fabrication, Pressure Vessel and Piping Division, June 17–21, ASME, San Antonio, TX, 1984.
[3] P.S. Follansbee, The Hopkinson bar, in: Mechanical Testing, Metals Handbook, vol. 8, 9th ed., American Society for Metals, Metals Park, Ohio, 1985, pp. 198–217.
[4] L.D. Berthoff, C.H. Karnes, Two-dimensional analysis of the split Hopkinson pressure bar system, J. Mech. Phys. Solids 23 (1975) 1–19.
[5] L.D. Berthoff, Feasibility of two-dimensional numerical analysis of the split-Hopkinson bar system, J. Appl. Mech. 41 (1974) 137–144.
[6] Z. Tang, L. Wang, Computational data processing system of SHPB, Explosion Shockwaves 6 (4) (1986) 320–327.
[7] H. Zhao, G. Gary, J.R. Klepaczko, On the use of a viscoelastic split Hopkinson pressure bar, Int. J. Impact Eng 19 (4) (1997) 319–330, http://dx.doi.org/10.1016/S0734-743X(96), 00038-3.
[8] Q.M. Li, H. Meng, About the dynamic strength enhancement of concrete-like materials in a split Hopkinson pressure bar test, Int. J. Solids Struct. 40 (2003) 343–360, http://dx.doi.org/10.1016/S0020-7683(02)00526-7.
[9] W. Chen, B. Song, D.J. Frew, M. Forrestal, Dynamic small strain measurements of a metal specimen with a split Hopkinson bar, Exp. Mech. 43 (2003) 20–23, http://dx.doi.org/10.1007/BF02410479.
[10] S.N. Nasser, J.Y. Choi, W.G. Guo, et al., Very high strain-rate response of a Ni-Ti shape-memory alloy, Mech. Mater. 37 (2005) 287–298, http://dx.doi.org/10.1016/j.mechmat.2004.03.007.
[11] D.J. Frew, M.J. Forrestal, W. Chen, Pulse shaping techniques for testing brittle materials with a split Hopkinson pressure bar, Exp. Mech. 42 (2002) 93–106, http://dx.doi.org/10.1007/BF02411056.
[12] K. Xia, W. Yao, Dynamic rock tests using split Hopkinson (Kolsky) bar system, J. Rock Mech. Geotech. Eng. 7 (1) (2015) 27–59, http://dx.doi.org/10.1016/j.jrmge.2014.07.008.
[13] B.A. Gama, S.L. Lopatnikov, J.W. Gillespie Jr., Hopkinson bar experimental technique: a critical review, Appl. Mech. Rev. 57 (4) (2004) 223–250, http://dx.doi.org/10.1115/1.1704626.
[14] S. Sarva, A.D. Mulliken, Boyce, The mechanics of large-strain inhomogeneous deformation of polymeric materials under dynamic loading conditions, J. Phys. IV (Proc.) France 134 (2006) 95–101, http://dx.doi.org/10.1051/jp4:2006134016.
[15] R.J. Christensen, S.R. Swanson, W.S. Brown, Split Hopkinson bar tests on rock under confining pressure, Exp. Mech. 12 (1972) 508–541.
[16] X.B. Li, T.S. Lok, J. Zhao, P.J. Zhao, Oscillation elimination in the Hopkinson bar apparatus and resultant complete dynamic stress-strain curves for rocks, Int. J. Rock Mech. Min. Sci. 37 (2000) 1055–1060, http://dx.doi.org/10.1016/S1365-1609(00)00037-X.
[17] X.B. Li, T.S. Lok, J. Zhao, Dynamic characteristics of granite subjected to intermediate loading rate, Rock Mech. Rock Eng. 38 (1) (2005) 21–39, http://dx.doi.org/10.1007/s00603-004-0030-7.
[18] S. Ellwood, L.J. Griffiths, D.J. Parry, Materials testing at high constant strain rates, J. Phys. E: Sci. Instrum. 15 (1982) 280–282.
[19] D.J. Parry, A.G. Walker, P.R. Dixon, Hopkinson bar pulse smoothing, Meas. Sci. Technol. 6 (1995) 443–446, http://dx.doi.org/10.1088/0957-0233/6/5/001.
[20] M.J. Forrestal, D.J. Frew, W. Chen, The effect of sabot mass on the striker bar for split Hopkinson pressure bar experiments, Exp. Mech. 42 (2002) 129–131, http://dx.doi.org/10.1007/BF02410873.
[21] H. Yang, H. Song, S. Zhang, Experimental investigation of the behavior of aramid fiber reinforced polymer confined concrete subjected to high strain-rate compression, Constr. Build. Mater. 95 (2015) 143–151, http://dx.doi.org/10.1016/j.conbuildmat.2015.07.084.
[22] Z. Deng, H. Cheng, H. Wang, G. Zhu, H. Zhong, Compressive behavior of the cellular concrete utilizing millimeter-size spherical saturated SAP under high strain-rate loading, Constr. Build. Mater. 119 (2016) 96–106, http://dx.doi.org/10.1016/j.conbuildmat.2016.05.018.
[23] R. Naghdabadi, M. Ashrafi, J. Arghavani, Experimental and numerical investigation of pulse shaped split Hopkinson pressure bar test, Mater. Sci. Eng. A 539 (2012) 285–293. http://dx.doi:10.1016/j.msea.2012.01.095.
[24] W. Yonghua, W. Zhengdao, L. Xiaoyan, A. Minzhe, Experimental and numerical studies on dynamic compressive behavior of reactive powder concretes, Acta Mech. Solida Sin. 21 (5) (2008) 420–430. http://dx.doi:10.1007/s10338-008-0851-0.
[25] X.D. Chen, S.X. Wu, J.K. Zhou, Experimental and modeling study of dynamic mechanical properties of cement paste, mortar and concrete, Constr. Build. Mater. 47 (2013) 419–430, http://dx.doi.org/10.1016/j.conbuildmat.2013.05.063.
[26] W. Li, J. Xu, Impact characterization of basalt fiber reinforced geopolymeric concrete using a 100-mm-diameter split Hopkinson pressure bar, Mater. Sci. Eng. A 513–514 (2009) 145–153, http://dx.doi.org/10.1016/j.msea.2009.02.033.
[27] X. Luo, J. Xu, E. Bai, W. Li, Research on the dynamic compressive test of highly fluidized geopolymer concrete, Constr. Build. Mater. 48 (2013) 166–172, http://dx.doi.org/10.1016/j.conbuildmat.2013.06.035.
[28] J. Zhou, X. Chen, L. Wu, X. Kan, Influence of free water content on the compressive mechanical behavior of cement mortar under high strain rate, Sadhana-Acad. Proc. Eng. Sci. 36 (3) (2011) 357–369, http://dx.doi.org/10.1007/s12046-011-0024-6.
[29] H. Su, J. Xu, W. Ren, Mechanical properties of ceramic fiber-reinforced concrete under quasi-static and dynamic compression, Mater. Des. 57 (2014) 426–434, http://dx.doi.org/10.1016/j.matdes.2013.12.061.
[30] M.A. Meyers, Dynamic Behavior of Materials, Wiley, New York, 1994.
[31] W.N. Chen, B. Song, Split Hopkinson (Kolsky) Bar, Springer Press, New York, 2011, p. 87.
[32] ASTM-International editor, ASTM Standards, ASTM C33/C33M-16, Standard specification for concrete aggregates, Annual Book of ASTM Standards, ASTM International, West Conshohocken, PA, 2016.
[33] ASTM-International editor, ASTM Standards, ASTM C494/C494M-15a, Standard specification for chemical admixtures for concrete, Annual Book of ASTM Standards, ASTM International, West Conshohocken, PA, 2015.
[34] Y. Hao, H. Hao, Z.X. Li, Influence of end friction confinement on impact tests of concrete material at high strain rate, Int. J. Impact Eng 60 (2013) 82–106, http://dx.doi.org/10.1016/j.ijimpeng.2013.04.008.
[35] ASTM-International editor, ASTM Standards, ASTM C39/C39M-16: Standard test method for compressive strength of cylindrical concrete specimens, Annual Book of ASTM Standards, ASTM International, West Conshohocken, PA, 2016.
[36] ASTM-International editor, ASTM Standards, ASTM C469/C469M-14, Standard test method for static modulus of elasticity and Poisson's ratio of concrete in compression, Annual Book of ASTM Standards, ASTM International, West Conshohocken, PA, 2014.
[37] ACI Committee 318, Building Code Requirements for Structural Concrete (ACI 318-14) and Commentary (318R-14), American Concrete Institute, Farmington Hills, 2014.
[38] D.L. Grote, S.W. Park, M. Zhou, Dynamic behavior of concrete at high strain rates and pressures: I. Experimental characterization, Int. J. Impact Eng 25 (9) (2001) 869–886, http://dx.doi.org/10.1016/S0734-743X(01)00020-3.
[39] S.S. Wang, M.H. Zhang, S.T. Quek, Mechanical behavior of fiber-reinforced high-strength concrete subjected to high strain-rate compressive loading, Constr. Build. Mater. 31 (6) (2012) 1–11, http://dx.doi.org/10.1016/j.conbuildmat.2011.12.083.
[40] LS-DYNA key word user's manual, Volume II (material models), Version R7.0, Livermore Software Technology Corporation (LSTC).
[41] T.J. Holmquist, G.R. Johnson, W.H. Cook, A computational constitutive model for concrete subjected to large strains, high strain rates and high pressures, in: Proceedings 14th International Symposium on Ballistics, Quebec, Canada, 1993, pp. 591–600.
[42] Y.S. Tai, C.C. Tang, Numerical simulation: the dynamic behavior of reinforced concrete plates under normal impact, Theoret. Appl. Fract. Mech. 45 (2006) 117–127, http://dx.doi.org/10.1016/j.tafmec.2006.02.007.
[43] K.S. Vecchio, F. Jiang, Improved pulse shaping to achieve constant strain rate and stress equilibrium in split-Hopkinson pressure bar testing, Metall. Mater. Trans. A 38A (2007) 2655–2665, http://dx.doi.org/10.1007/s11661-007-9204-8.
[44] A.G. Bazle, Split Hopkinson pressure bar technique: experiments, analyses and applications, United States, the Faculty of the University of Delaware, spring, 2004.
[45] X. Zhang, G. Ruiz, R.C. Yu, E. Poveda, P. Porras, Rate effect on the mechanical properties of eight types of high-strength concrete and comparison with FIB MC2010, Constr. Build. Mater. 30 (2012) 301–308, http://dx.doi.org/10.1016/j.conbuildmat.2011.11.037.
[46] O.S. Lee, S.H. Kim, Y.H. Han, Thickness effect of pulse shaper on dynamic stress equilibrium and dynamic deformation behavior in the polycarbonate using SHPB technique, Exp. Mech. 21 (1) (2006) 51–60.
[47] Y. Zhou, J. Zhao, Advances in Rock Dynamics and Applications, CRC Press, Taylor & Francis group, London, UK, 2001.